https://doi.org/10.5194/nhess-2023-44
Preprint. Discussion started: 13 April 2023

Natural Hazards and Earth System Sciences
Discussions

Non-landslide sampling and ensemble learning techniques to improve landslide susceptibility mapping

Chao Zhou [1, 2, 3], Yue Wang [2, 4], Ying Cao [2, 4] *, Ramesh P. Singhc [5], Bayes Ahmed [6], Mahdi Motagh [3, 7], Yang Wang [2, 4], Ling Chen [2, 4]

[1] School of Geography and Information Engineering, China University of Geosciences, Wuhan 430078, China
[2] Research Center of Geohazard Monitoring and Warning in the Three Gorges Reservoir, Chongqing 40400, China
[3] Department of Geodesy, Section of Remote Sensing and Geoinformatics, Helmholtz Centre Potsdam, GFZ German Research Centre for Geosciences, Potsdam 14473, Germany
[4] Engineering Faculty, China University of Geosciences, Wuhan 430074, China
[5] School of Life and Environmental Sciences, Schmid College of Science and Technology, Chapman University, Orange, CA, USA
[6] Institute for Risk and Disaster Reduction, University College London (UCL), London WC1E 6BT, UK
[7] Institute for Photogrammetry and Geoinformation, Leibniz University Hannover, Hannover 30167, Germany

Correspondence: Ying Cao (caoying@cug.edu.cn)

Abstract: In recent years, several catastrophic landslide events have been observed throughout the globe, significantly affecting the loss of lives, infrastructure, everyday life and livelihood. To minimize the impact of landslides and issue early warnings, landslide susceptibility maps (LSM) are essential. Aim to improve the accuracy of LSM, this study applied a random selection of non-landslide samples and low accuracy of individual classifiers using machine learning (ML) techniques, coupled with ensemble learning and ML, for LSM. China's Zigui-Badong section of the Three Gorges Reservoir area (TGRA) was considered a case study. Twelve influencing factors were selected as inputs for modelling, and the relationship between each causal factor and landslide spatial development was quantitatively analyzed. A total of 179 landslides were identified in the present study. About 70% of the landslide pixels were randomly considered for training, and the remaining 30% were used for validation. The Logistic Regression model (LR) was applied to produce an initial susceptibility map, and the non-landslide samples were selected within the classified low-susceptibility area. Subsequently, two ML classifiers – the Classification and Regression Tree (CART), and the Multi-Layer Perceptron (MLP), and four coupling models – the CART-Bagging, CART-Boosting, MLP-Bagging, and MLP-Boosting, were utilized for LSM. Finally, the receiver operating characteristics (ROC) curve and statistical analysis were applied for accuracy assessment. The results show that elevation and distance to rivers were the main causal factors of landslide development in the study area. The modeling accuracy of LR-MLP was calculated approx. 0.901, which is higher than the LR-CART (0.889). The LR-MLP-Boosting performed the best with an accuracy of 0.986 followed by the LR-CART-Bagging (0.973), LR-CART-Boosting (0.981), and LR-MLP-Bagging (0.978). The accuracy has been improved compared with the NO-

https://doi.org/10.5194/nhess-2023-44
Preprint. Discussion started: 13 April 2023

CART, NO-MLP, NO-CART-Bagging, NO-CART-Boosting, NO-MLP-Bagging, and NO-MLP-Boosting models. Four ensemble models outperformed their corresponding classifiers, while Boosting outperforms Bagging. Overall, the combination of ensemble learning and ML effectively improved the accuracy of LSM. The LR model can effectively constrain the selection range of non-landslide samples and enhance the quality of sample selection. Our results show promise to map susceptible landslides locations which will help to monitor for an early warning of the landside.

Keywords: Reservoir landslide; susceptibility mapping; non-landslide sampling; ensemble learning; machine learning; Three Gorges Reservoir Area

1 Introduction

Landslides are severe, sudden, and frequent geological disasters that occur throughout the globe, significantly affecting the loss of life, infrastructure, and economic conditions. The Ministry of Natural Resources of China reported that 4,810 landslide disasters occurred in 2020, resulting in 139 deaths and 730 million US dollars in direct economic losses. The Three Gorges Reservoir area (TGRA) is a highly landslide-prone area, with more than 5,000 landslide occurrences recorded (Yin et al, 2022). During the first impoundment of the TGRA in July 2003, the Qianjiangping landslide caused a death toll of 24 and an economic loss of about 11.6 million US dollars (Tang et al., 2019). Landslide risk assessment has been widely used as a vital means of disaster prevention and mitigation (Xie et al., 2019). It is the foundation for quantitative risk assessment and the final land-use map and planning map. However, due to the nonlinear relationship between landslide occurrence and their influencing factors, accurate landslide susceptibility modeling (LSM) is challenging for geoscientists and engineers.

Over the past few decades, LSM methods have been developed for qualitative and quantitative evaluation of landslide-prone areas (Sabokbar et al., 2014; Zhou et al., 2015). In the qualitative method, the weight of various controlling parameters is determined by experts based on past experience. This method requires landslide-vulnerable areas based on past landslide events, geology, and slope. The qualitative methods include expert scoring and analytic hierarchy methods based on numerous controlling landslide parameters (Kayastha et al., 2013; Yu et al., 2022; Meena et al., 2022; Roy et al., 2023). The quantitative method is divided based on data and physical driven parameters. With the development of earth observation techniques, data quality, such as landslide catalogues and topographic landforms, has been significantly improved, making the data-driven method popular in LSM. The machine learning (ML) technique has a strong nonlinear fitting ability and has been applied in various fields. The ML methods include support vector

https://doi.org/10.5194/nhess-2023-44
Preprint. Discussion started: 13 April 2023

machines (Huang and Zhao, 2018; Huang et al., 2018; Chen et al., 2017), decision trees (Yang et al., 2019), and neural networks (Zhou et al., 2018; Huang et al., 2016; Huang et al., 2017). Machine learning methods are reported to outperform traditional methods in LSM (Lin et al., 2020; Zheng et al., 2020; Chen et al., 2020; Bui et al., 2019).

For the unbalanced sample composed of a large proportion of non-landslides and small landslides, there are problems with having LSM. The single ML classifier cannot perform satisfactorily when dealing with unbalanced samples (Tanyu et al., 2021; Long et al., 2021; Yan et al., 2022). Ensemble learning is an effective method to solve the classification problem of sample imbalance. This technique strategically creates multiple models and combines them to produce improved performance. After introducing this method, the ensemble learning techniques (Pham et al. 2019) gained much attention from the research community for natural hazard modeling. Recently, ensemble learning has been applied in LSM, and some impressive results have been achieved (Zhou et al., 2020; Di Napoli et al., 2020; Pham et al., 2020; Fang et al., 2021; Lv et al., 2022). However, we have not agreed on the modeling framework applying ML and ensemble learning coupled techniques for LSM.

The selection of machine learning training samples is vital to the accuracy of LSM. Since the number of non-landslide samples is much larger than that of landslide samples, the accurate LSM is the selection of effective training samples under unbalanced dataset conditions (Fang et al., 2021). However, most existing studies subjectively and/or randomly select the non-landslide samples from whole landslide-free areas (Huang et al., 2020). Therefore, the geological condition of selected non-landslide samples using this method may be similar to the landslide development area, which would affect the accuracy of LSM. At present, establishing an effective non-landslide sample selection method to ensure that the selected non-landslide samples have low susceptibility is still an urgent problem to be solved in ML-based LSM.

The Zigui-Badong geological section is located at the head area of the TGRA (Fig. 1). In the present study, we have considered this section for the detailed landslide susceptibility study. In the recent two decades, the precipitation and the periodic water level fluctuations in the reservoir have caused numerous landslides. Twelve controlling landslide factors are statistically analyzed and selected as inputs for modeling. An initial landslide susceptibility map is produced using Logical Regression (LR), and the non-landslide training samples are selected in the low susceptibility area. Two single models, namely Classification and Regression Tree (CART), Multi-Layer Perceptron (MLP), and four coupling models (CART-Bagging, CART-Boosting, MLP-Bagging, and MLP-Boosting) were utilized for LSM. Finally, the modeling performance is compared

https://doi.org/10.5194/nhess-2023-44
Preprint. Discussion started: 13 April 2023

by Receiver Operating Characteristic (ROC) Curve and statistical analysis method. Our results encourage establishing a high-accurate susceptibility model for reservoir landslides in the TGRA.

2 Study area

The study area is located in the first section of the Three Gorges Reservoir, spanning Zigui and Badong counties. The longitude and latitude ranges are 30°51’-31°4’ N, 100°17’-100°52’ E, and the total area is about 656 km^2 (Fig. 1). It is a high-prone area for landslide disasters with an altitude range of 80 - 2, 020 m. The geological structure in the study area is complex, with developed faults and fragmented rock mass. Triassic and Jurassic dominate the stratum, and the lithology is mostly carbonate, sand shale, marlstone, and mudstone, which is sensitive to landslide development. Quaternary is widely exposed in the study area and accumulates on the terraces and slope surfaces. In addition, the study area has excessive rainfall, with an average annual rainfall of 1,250 mm, mainly during May-September.

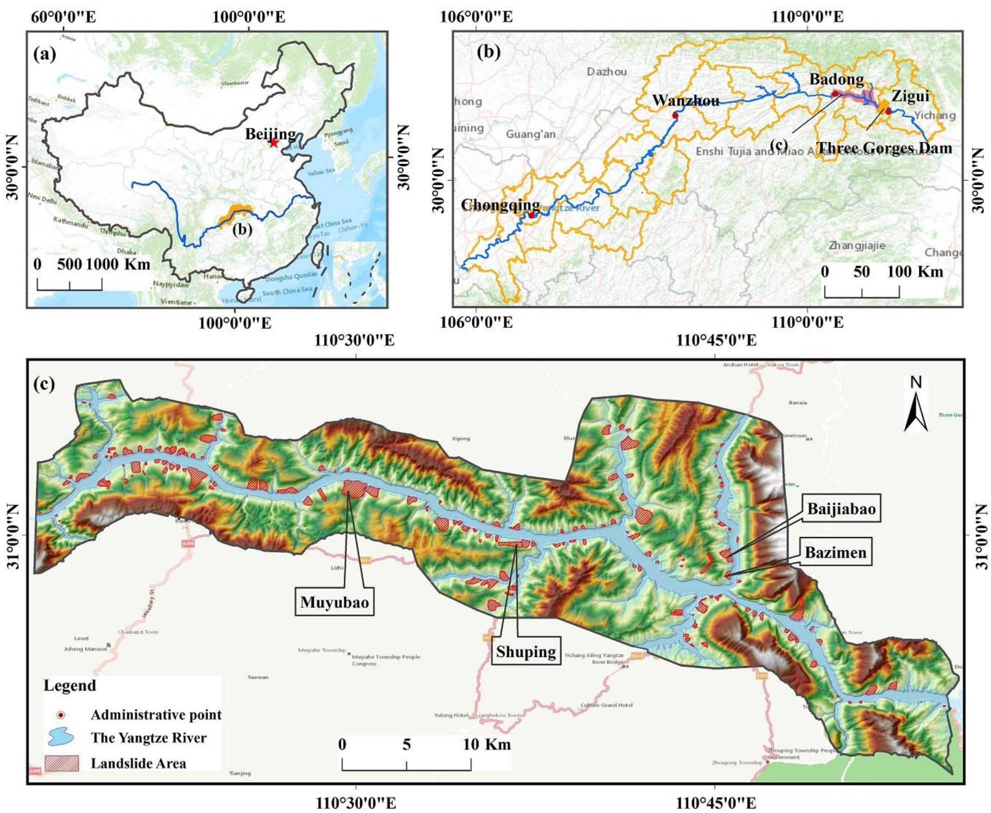

Fig. 1: (a) Map of China, (b) Map of the Three Gorges Reservoir area, and (c) Topography and landslide distribution in the study area. The background maps are collected from ArcGIS Online.

In 2003, the TGRA was first impounded up to 135 m. After September 2008, the reservoir water level periodically fluctuates between 145 m - 175 m per year, significantly changing the bank slope's hydrogeological conditions (Zhou et al., 2016; Ye et al., 2021; Yin et al, 2021). The reservoir water level fluctuation significantly affected the bank slope's original balance. It induced the deformation or failure of a large number of reservoir landslides, such as the Qianjiangping landslide (Wang et al., 2008), the Muyubao landslide (Zhou et al., 2020), and the Shuping landslide (Zhou et al., 2018).

3 Methodology

3.1 Procedure for LSM

The LSM procedure includes four parts: influencing factor selection and landslide pixel sampling, non-landslide pixel sampling, model construction, and accuracy evaluation (Fig. 2). a). We have considered the influencing factors for LSM; 70% of the landslide pixels were selected as the training data, while the remaining 30% was applied for validation; b) We produce a preliminary susceptibility map using LR and non-landslide pixels with an equal number of landslide pixels are randomly selected in the low susceptibility area; c) Two single models (CART and MLP) and four coupling models (CART-bagging, CART-boosting, MLP-bagging, and MLP-boosting,) are applied for LSM; d) We use statistical analysis method and ROC curves to evaluate the partitioning results and model performance.

https://doi.org/10.5194/nhess-2023-44
Preprint. Discussion started: 13 April 2023

Natural Hazards and Earth System Sciences
Open Access
EGU
Discussions

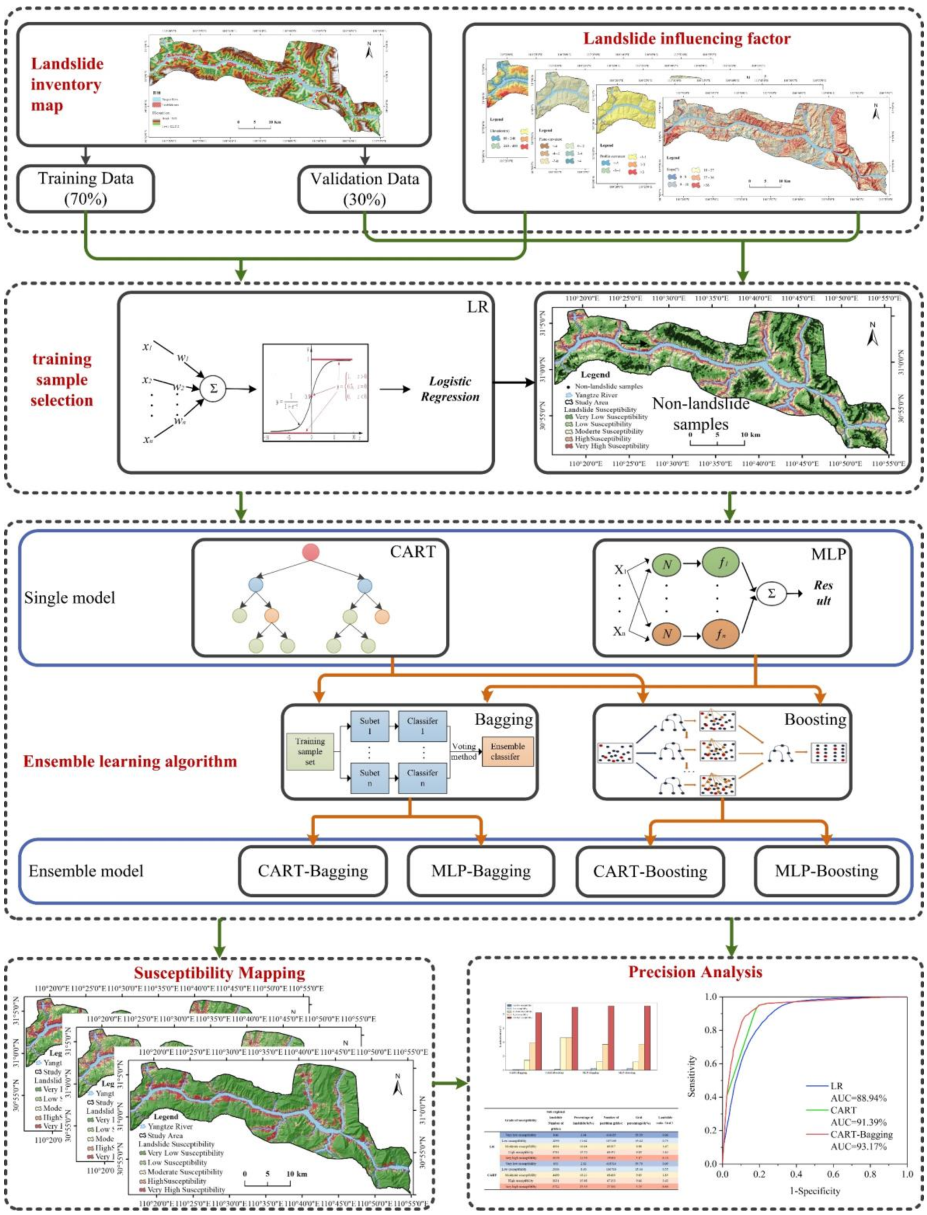

Fig. 2 The flowchart of the landslide susceptibility mapping.

3.2 Information value method

Information value is a statistical method based on information theory, which can calculate the impact of different factors on the occurrence of landslides. In LSM, the formula of information value can be given as follows:

$$I_i = \sum_{i=1}^{n} Ln \frac{S_i/S}{A_i/A} \tag{1}$$

https://doi.org/10.5194/nhess-2023-44
Preprint. Discussion started: 13 April 2023

Natural Hazards and Earth System Sciences
Discussions

Where I_i is the information value of the i-th influencing factor; S_i is the number of landslide pixels within the i-th influencing factor; S is the total number of landslide pixels; A_i is the number of pixels for the i-th influencing factor; A is the total number of pixels in the study area; n is the number of influencing factors (Zhou et al., 2018). When the information value is greater than 0, the factor promotes the occurrence of landslides. Conversely, when the value is less than 0, it indicates that the factor inhibits the occurrence of landslides. Moreover, the larger the absolute information value, the stronger the effect.

3.3 Classifier

3.3.1 Multi-Layer Perceptron

Multi-Layer Perceptron (MLP) is a feed-forward artificial neural network widely used in many fields. It consists of three layers: input layer, hidden layer, and output layer (Fig. 3). MLP with a sufficient number of hidden layer neurons can realize any nonlinear mapping from *n*-dimensional to *m*-dimensional (Gardner and Dorling, 1998). During the calculation process, the input layer neurons receive sample data, and the hidden layer and the output layer neurons deal with the inputs according to the weight value. To build a better model, MPL modifies the weight value through backpropagation. The learning process of MPL models is constantly adjusting the parameters. The training of the MPL model is the process of constantly adjusting network parameters.

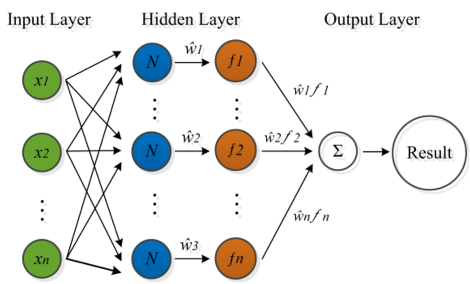

Fig. 3 MLP neural network structure.

3.3.2 Classification and Regression Tree

Classification and Regression Tree (CART) is a simple but powerful approach to forecasting an event (Breiman, 1984). This method is easy to understand and implement for LSM. During modeling, CART does not need to presuppose a relationship between the predictor and target variables. The child nodes are obtained to form a binary tree by recursively dividing the data set. The child nodes are continuously expanded to generate a complete decision tree and perform the necessary pruning to prevent overfitting. The Gini index minimization criterion determines the optimal segmentation point, and the smaller the Gini index is, the better the effect of tree division. The Gini index represents the classification error rate for the binary classification problem. For example, if the sample set D contains k categories, the Gini coefficient of the sample set can be expressed as:

$$Gini(D) = 1 - \sum_{i=1}^{k}(\frac{C_i}{D})^2 \quad (2)$$

where C_i is a subset of class i samples in D.

3.3.3 Logical Regression

The logical regression (LR) model is a statistical analysis model suitable for binomial categorical dependent variables. It is widely used in landslide prediction due to its simple operation and relatively accurate (Youssef et al., 2016). Training testing on known landslide events establishes the nonlinear relationship between the dependent variable and multiple independent variables. Therefore, the occurrence probability of future landslides can be predicted or evaluated using the established formula. The method takes the landslide influencing factor as the independent variable and the occurrence probability of landslides as the dependent variable (landslide is 1, the non-landslide is 0). The independent variable can be continuous or discrete. Assuming that the probability of landslide occurrence is P, the regression equation can be written as follows:

$$P = \frac{1}{1+e^{-(b_0+b_1x_1+b_2x_2+\ldots+b_nx_n)}} \quad (3)$$

where b_0 is a constant, n is the number of independent variables, x_1, x_2,..., x_n is the landslide influencing factors, and b_1, b_2,..., b_n are the coefficients of LR.

3.4 Ensemble learning

3.4.1 Boosting

Boosting algorithm is a process of enhancing a simple weak classification algorithm to reduce variance and bias through iterative training and improve the ability to classify model data (Youssefa et al., 2016). Boosting algorithm generates a classifier combination through multiple iterations. Each iteration constructs a new training set from a sample returned to the total dataset. And each iteration will adjust the weight of the sample so that the error samples get higher weight values at the next iteration. After T iterations, the updated weak classifiers are weighted and superimposed to obtain the strong classifier (Fig. 4).

https://doi.org/10.5194/nhess-2023-44
Preprint. Discussion started: 13 April 2023

Natural Hazards and Earth System Sciences
Open Access
Discussions

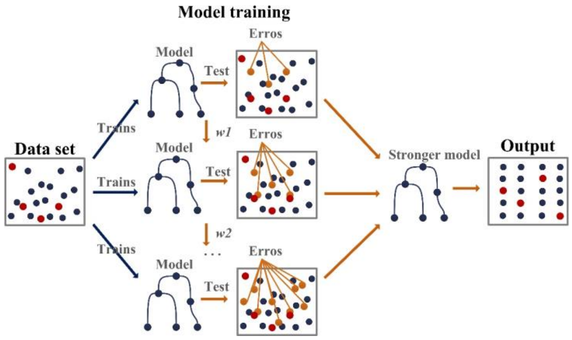

Fig. 4 Schematic diagram of Boosting ensemble algorithm.

3.4.2 Bagging

The Bagging algorithm is an ensemble learning method proposed in 1996 (Breiman et al., 1996). Its core idea is to repeat the input training sets by Bootstrap sampling to obtain *n* subsets and build a weak classifier for each subset. The voting method integrates the weak (n) classifiers to form a strong classifier. The Bagging algorithm can observe small changes in the training data, effectively improving the accuracy and stability of the model prediction results, especially for models susceptible to sample disturbances (Fig.5).

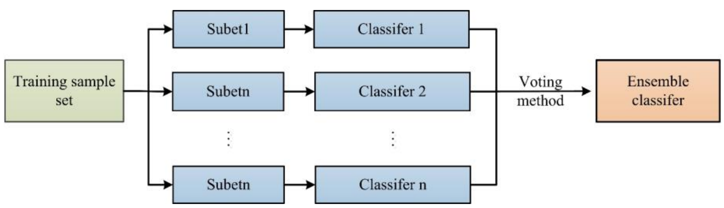

Fig. 5 Flowchart showing the Bagging ensemble algorithm.

4 Modelling and results

4.1 Landslide inventory and data preparation

Accurate and reliable landslide inventory data is essential for LSM. This study prepared the landslide inventory using field data, historical landslide inventory, and high-resolution remote sensing images. The data source of this study includes: (a) a topographic map (1:10,000) for extraction of topography, landscape, and rivers; (b) a geological map (1:50,000) for extraction of lithology, geologic structure, faults, and so on; (c) field investigation data; and (d) the historical landslide inventory. A total of 179 landslides are identified in the study area, distributed in spots or bands along the Yangtze River (Fig. 1). The total area of the identified landslides is 22.14 km^2. In contrast, the area of individual landslides ranges from 0.13 km^2 to 1.80 km^2. There are four typical reservoir landslides: Baijiabao landslide, Shuping landslide, Bazimen landslide, and Muyubao landslide (Fig. 6).

https://doi.org/10.5194/nhess-2023-44
Preprint. Discussion started: 13 April 2023

Natural Hazards and Earth System Sciences
Discussions

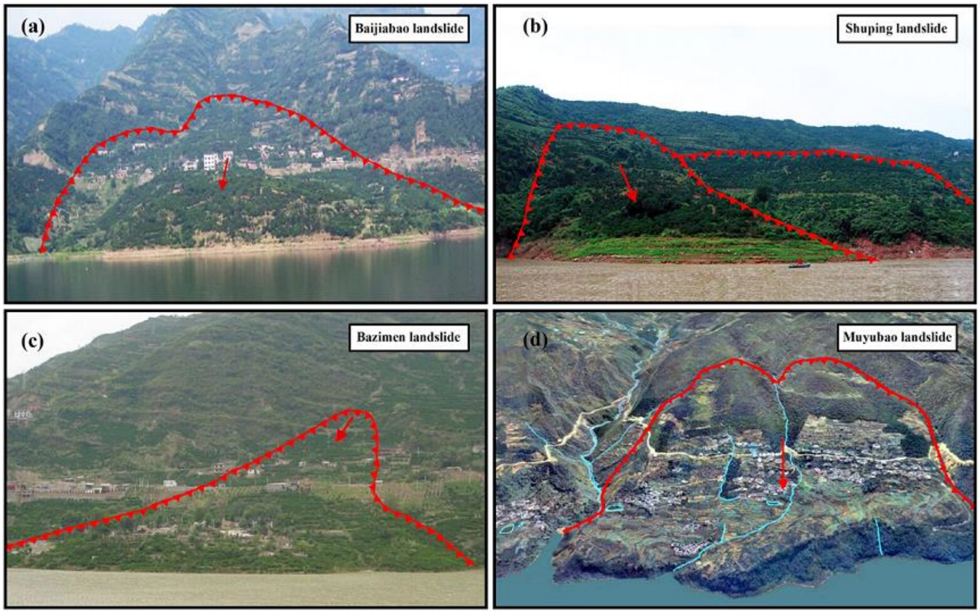

Fig. 6 Typical reservoir landslides in the Three Gorges Reservoir area. The locations are shown in Fig. 1.

4.2 Landslide influencing factors

Different influencing factors cause landslide occurrence in various regions due to the diverse geological environments. With the consideration of the regional geological conditions, landslide inventory, and earlier studies (Yu et al., 2016; Li et al., 2020; Yu et al., 2021), twelve influencing factors were prepared initially for LSM, namely altitude, slope, aspect, terrain roughness index (TRI), topographic relief, slope geometry, slope structure, lithology, topographic wetness index (TWI), land use, distance to rivers, and distance to faults. According to the Technical requirement for the geo-hazard survey (1:50,000) of China Geological Survey, the raster of 30 m×30 m is adopted as the basic unit for LSM. All layers of twelve influencing factors are extracted in *ArcGIS 10.2*.

4.2.1 Altitude

Many activities, roads, bridges, and infrastructures occur at low altitudes in the study area. With such activities, the stability of natural slopes is easily damaged; with the excessive rainfall in landslide-prone areas, slope failure often causes landslides. The altitude of this study area varies 145~2,020 m, which is divided into five classes: [145 ~ 240), [240 ~ 450), [450 ~ 650), [650 ~ 1200), [1200 ~ 2020) (Fig. 7a). As suggested in Table 1, landslides in this study area mainly occurred in the altitude range of 145~240 m, the information value of which is the highest of 1.49. No landslide occurred in the region with an altitude of more than 1200 m since the slope is not disturbed.

https://doi.org/10.5194/nhess-2023-44
Preprint. Discussion started: 13 April 2023

Table 1 Statistics between causal factors and landslides occurrence.

Causal factor	Category	IV	Causal factor	Category	IV
Slope (°)	0~9	-0.90	Aspect	flat	-1.93
	9~18	0.37		north	0.47
	18~27	0.42		northeast	0.23
	27~36	-0.28		east	-0.27
	>36	-1.63		southeast	-0.31
TRI	1~1.1	0.37		south	0.43
	1.1~1.2	-0.04		southwest	-0.29
	1.2~1.3	-0.88		west	-0.71
	1.3~1.4	-1.9		northwest	-0.03
	1.4~1.5	-2.48	Distance to faults (m)	0-500	-0.04
	>1.5	-2.49		500-1,000	0.08
Distance to rivers (m)	0~300	0.92		1,000-1,500	0.24
	300~600	0.29		1,500-2,000	0.23
	600~900	-0.57		> 2,000	-0.22
	900~1,200	-1.7	Altitude (m)	<240	1.49
	>1,200	-2.95		240-450	0.54
Lithology	L1	-3.94		450-650	-1.36
	L2	-0.3		650-1,200	-3.84
	L3	0.17		>1,200	-∞
	L4	-0.34	Slope geometry	X/X	0.16
	L5	0.42		X/V	-0.96
TWI	1.37~3	-2.49		X/GE	-1.45
	3~4.5	-0.37		V/X	0.04
	4.5~6	-0.20		V/V	-1.74
	6~7.5	0.47		V/GE	-1.19
	7.5~9	0.72		GR/X	0.01
	>9	0.02		GR/V	-1.02
Topographic relief (m)	0-14	-0.63		GR/GE	-1.46
	14-35	0.47	Slope structure	B1	-∞
	35-42	0.08		B2	0.14
	42-49	-0.47		B4	0.13
	>49	-1.70		B5	0.08
Land use	Mountain land	-0.59		B6	-0.17
	Farmland	0.12		B7	-0.34
	Waterbody	0.43		B8	-0.67
	Construction land	0.85			

Note: IV refers to Information Value; The meaning of the lithology, slope structure, and slope type abbreviation of the formation is shown in Tables 2, 3 and 4.

4.2.2 Slope

The slope affects the stress distribution, materials accumulation, and surface runoff. It can be divided into five classes: very gentle [0, 9°], gentle (9°, 18°], moderate (18°, 27°], steep (27°, 36°], and very steep (36°, 90] (Fig. 7b). Landslides generally occur in the gentle slope, whose information value is 0.42. When the slope is more than 36°, the occurrence of a landslide is significantly inhibited, and the information value is the lowest of -1.63.

4.2.3 Aspect

Rainfall and sunlight exposure varies with aspect. It leads to the differences in physical and mechanical properties of sliding masses, which leads to differences in landslide stability. (Pham et al., 2021). The aspect

https://doi.org/10.5194/nhess-2023-44
Preprint. Discussion started: 13 April 2023

in this study was divided into nine categories. The landslides with north and northeast aspects are the easiest to occur; their information value is 0.47 and 0.23, respectively (Fig. 7c).

4.2.4 Topographic relief

The relief shows the relative height difference within the study area. The calculation formula of the relief factor is shown as follows (Liu et al., 2009):

$$D = Hmax - Hmin \tag{4}$$

Where, D is the relief factor; *Hmax* is the highest altitude value; *Hmin* is the lowest altitude value. The topographic relief in this study is divided into five classes: [0 ~ 14 m), [14 ~ 35 m), [35 ~ 42 m), ⩾ 49 m (Fig. 7d). The information values are -0.63, 0.47, 0.08, -0.47 and -1.70, respectively.

4.2.5 Slope geometry

Slope curvature is the microscopic performance of the earth's surface landforms, divided into plane curvature and profile curvature. It reflects the concavity of the slope along the aspect, which controls the flow speed of surface material and rainfall confluence (Abdo et al., 2022). We classify the plane and profile curvatures into three categories respectively. The nine slope geometries are defined with the combination of plane and profile curvatures (Table 2, Fig. 7e). In this study area, landslides mainly occur in the slope type of X/X, with the highest value of 0.16.

Table 2 Definition for slope geometry classification.

Plan curvature / Profile curvature	Outward slope (X)	Inward slope (V)	Straight slope (GR)
Convex slope (X)	X/X	V/X	GE/X
Concave slope (V)	X/V	V/V	GE/V
Straight slope (GE)	X/GR	V/GR	GE/GR

4.2.6 Terrain Roughness Index

The terrain roughness index (TRI) reflects the degree of surface fluctuation and erosion. The calculation formula is shown as follows (Moore et al., 1991):

$$TRI = \sqrt{Abs(max^2 - min^2)} \tag{5}$$

The TRI is divided into six classes: [1~1.1), [1.1~1.2), [1.2~1.3), [1.3~1.4), [1.4~1.5), and ⩾1.5 (Fig. 7f). The information values are 0.37, -0.04, -0.88, -1.90, -2.48, and -2.49, respectively (Table 1).

4.2.6 Land use

Land use and landslide development are closely related to the triggering of landslides due to the changes in the slope. In our study area, land use is divided into four categories, namely water bodies, construction land, farmland, and mountain land (Fig. 7g). In the foothills and mountainous areas, land use and land cover are changing, affecting the slope that causes the triggering of the landslides. Further, the construction land is mainly concentrated in the gentle river terraces on both sides of the Yangtze River. A large number of

https://doi.org/10.5194/nhess-2023-44
Preprint. Discussion started: 13 April 2023

excavations, slope cutting, and other activities in the construction of houses and roads directly impact the slope's stability, and the information value is the highest of 0.85.

4.2.8 Slope structure

Slope structure indicates the intersection relationship between strata and slope, which determines the direction of the sedimentary stack on the slope. The slope structure in this study is divided according to Table 3 (Fig. 7h). In this study area, landslides mainly occurred in the B2 region. 35.06% of the total pixels are distributed in this category, whose information value is 0.42.

Table 3 Classification of slope structure (Zhou et al., 2018).

Category	Definition (slope: θ, aspect: σ, bed dip angle: α, bed dip direction: β)
B1	$a< 10^\circ$
B2	$((\lvert\alpha-\beta\rvert \in (0,30^\circ)\Vert(\lvert\alpha-\beta\rvert \in (330^\circ,360^\circ)))\&\&(\alpha>10^\circ)\&\&(\theta>\alpha)$
B3	$((\lvert\alpha-\beta\rvert \in (0,30^\circ])\Vert (\lvert\alpha-\beta\rvert \in (330^\circ,360^\circ)))\&\&(\alpha>10^\circ)\&\&(\theta=\alpha)$
B4	$((\lvert\alpha-\beta\rvert \in (0,30^\circ)\Vert(\lvert\alpha-\beta\rvert \in [330^\circ,360^\circ)))\&\&(\alpha>10^\circ)\&\&(\theta<\alpha)$
B5	$(\lvert\alpha-\beta\rvert \in [30^\circ,60^\circ)\Vert (\lvert\alpha-\beta\rvert \in (330^\circ,360^\circ))$
B6	$(\lvert\alpha-\beta\rvert \in (60^\circ,120^\circ)\Vert(\lvert\alpha-\beta\rvert \in [240^\circ,300^\circ))$
B7	$(\lvert\alpha-\beta\rvert \in [90^\circ, 150^\circ))\Vert(\lvert\alpha-\beta\rvert \in (210^\circ,240^\circ))$
B8	$(\lvert\alpha-\beta\rvert \in [120^\circ, 180^\circ))\Vert(\lvert\alpha-\beta\rvert \in [180^\circ,210^\circ))$

4.2.9 Lithology

We divide the lithology in the study area into five categories (Table 4 and Fig. 7i). In the stratiform structure containing weak strata, especially in the stratified clastic rocks and the carbonate rocks developed on the weak bedrock, the large and medium-sized landslides more formed, and its information value is 0.42. On the other hand, few landslides developed in the hard rocks, such as granite and diorite, with the information value being the lowest of -3.94.

Table 4 Lithological classification in this study area.

Category	Geologic group	Main Lithology
L1	δ_{2-1}, Pt	Granite and diorite
L2	Z, ε_1, ε_{2+3}, O, T_1j, T_2b_3	Limestone, Shale, Malmstone
L3	T_1d, T_2b_{4+5}, J_1x, J_2s, J_3s	Marl mudstone
L4	S, J_2x	Shale, Mudstone and Shi Ying Sandstone, Muddy Siltstone, etc.
L5	T_3s, $J_{1-2}n$, J_3p	Malmstone (Feldspar sandstone, Shi Ying Sandstone, etc.) with coal seam

4.2.10 Topographic Wetness Index

Topographic Wetness Index (TWI) reflects topography's influence on soil water saturation (Alnajjar et al., 1991). It can be calculated using the following formula:

$$TWI = ln(\frac{As}{tan\beta}) \tag{6}$$

Where, A_S is the upstream gathering area and β is the slope. The TWI is divided into six categories:

https://doi.org/10.5194/nhess-2023-44
Preprint. Discussion started: 13 April 2023

[1.37, 3), [3, 4.5), [4.5, 6), [6, 7.5), [7.5, 9), and (9,-∞] (Fig. 7j). When the TWI value is within the range of [7.5~9), it shows the most substantial positive influence on landslide occurrence, whose information value is the highest of 0.72.

4.2.11 Distance to rivers

This study area is obviously affected by the hydrogeological environment, whose main river system is the Yangtze River and its tributaries (Fig. 1). After the impoundment of the TGRA, the stability of the bank slopes is influenced by the periodical fluctuation of reservoir water level, river erosion, and softening effect. The factor of distance to rivers represents the intensity of its influence. We divide the distance to rivers into four classes, namely [0~300 m), [300 m~900 m), [900 m~1,200 m), and ⩾1,200 m (Fig. 7k). The maximum information value is 0.92 within the distance range of 300 m. With the distance increasing, the influence of the river system on landslides gradually weakened, and the information value decreased.

4.2.12 Distance to faults

Due to the severely broken rock mass, the area with intense tectonic movement is prone to landslide disasters. Minor faults are developed in the study area, and the distance to the faults represents the intensity of their influence. We divide the distance to faults into four categories, namely [0~500 m), [500~1,000 m), [1,000~1,500 m), [1,500~2,000 m), and ⩾2,000 m (Fig. 7l). Their information values are -0.04, 0.08, 0.24, 0.23, and -0.22, respectively.

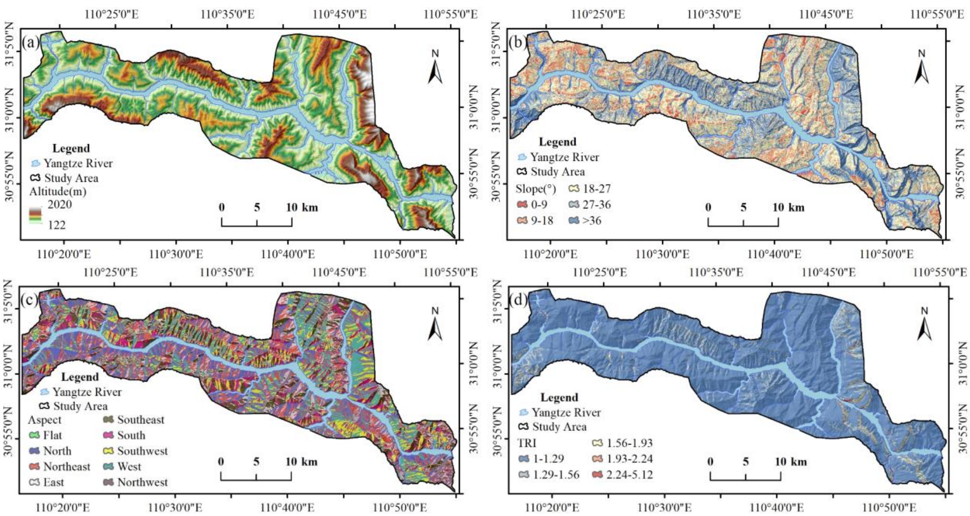

https://doi.org/10.5194/nhess-2023-44
Preprint. Discussion started: 13 April 2023

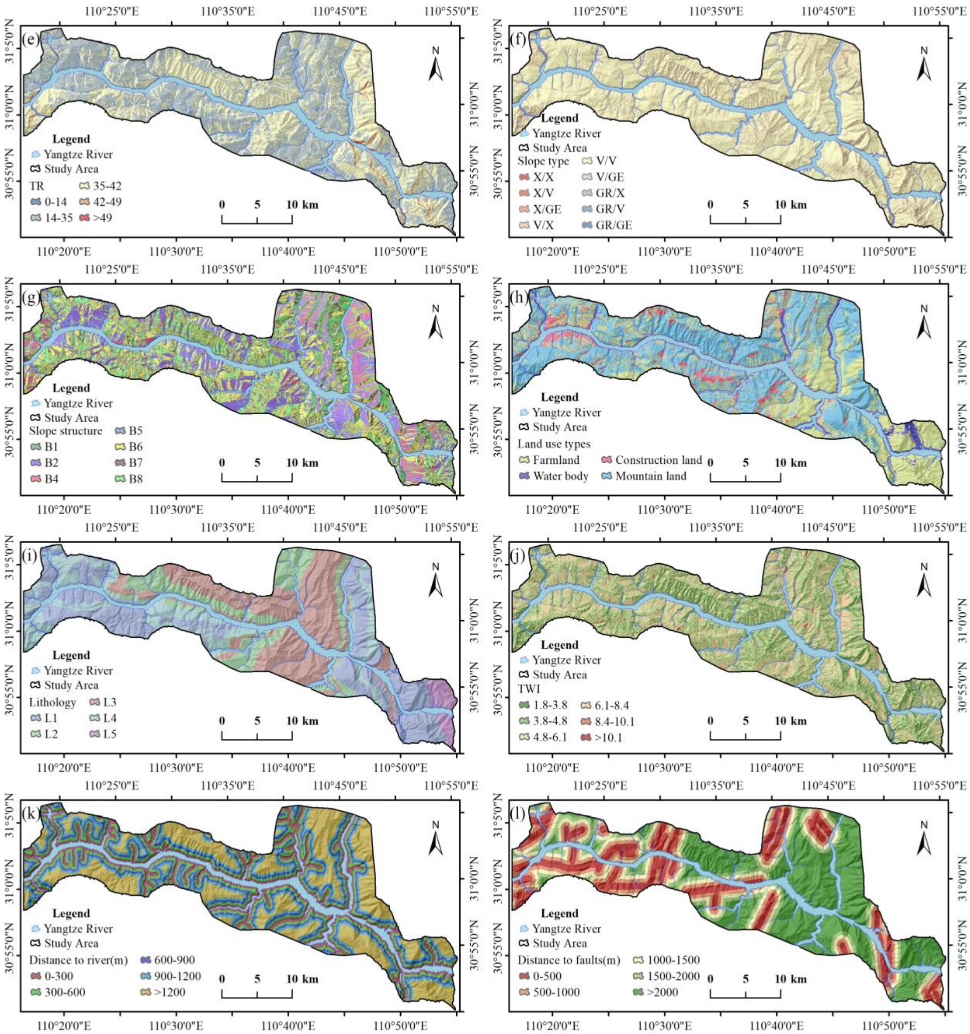

Fig.7 Shows various landslide factors: (a) Altitude, (b) Slope, (c) Aspect, (d) TRI, (e) Topographic relief, (f) Slope geometry, (g) Slope structure, (h) Land use, (I) Lithology, (j) TWI, (k) Distance to rivers, and (l) Distance to faults.

4.3 Landslide susceptibility modeling

4.3.1 Multi-collinearity analysis

The collinearity of factors will affect the performance of the evaluation model. Therefore, it is necessary to carry out a collinearity analysis before susceptibility modeling, to ensure that the factors are independent. The multi-collinear analysis is performed using Tolerance (T) and Variance Inflation Factor (VIF) (Zhou et al., 2018). When T is greater than 0.2 or VIF is less than 5, it is considered that there is no multi-collinearity between the factors. Both indices of T and VIF are calculated using *SPSS Statistics* 26.0, and the results are shown in Table 5. It indicates that all the twelve factors are independent with no collinearity.

https://doi.org/10.5194/nhess-2023-44
Preprint. Discussion started: 13 April 2023

Natural Hazards and Earth System Sciences
Open Access
EGU
Discussions

Table 5 Multi-collinearity analysis of the causal factors.

Influencing factors	T	VIF
Elevation	0.43	2.30
Slope	0.26	3.80
Aspect	0.96	1.04
Terrain Roughness Index	0.31	3.18
Topographic relief	0.32	3.12
Slope shape	0.64	1.52
Landuse	0.81	1.22
Slope structure	0.26	3.80
Stratigraphic lithology	0.94	1.06
Topographic Wetness Index	0.75	1.34
Distance to rivers	0.45	2.25
Distance to faults	0.95	1.05

4.3.2 Non-landslide sampling using LR

In this study, we randomly select 70% of landslide pixels for training and the remaining 30% for validation. Simultaneously, the same number of non-landslide samples are selected for model training. We propose a non-landslide sampling method to extract high-quality samples by the LR algorithm. At first, we produce a preliminary landslide susceptibility map by randomly selecting non-landslide as an example in landslide-free areas, using the following equations:

$$Logit(P) = -10.87 + 2.175 \bullet x_1 + 1.17 \bullet x_2 + 6.028 \bullet x_3 + 1.079 \bullet x_4 + 0.750 \bullet x_5 + 1.071 \bullet x_6 + 0.987 \bullet x_7 + 0.600 \bullet x_8 - 1.263 \bullet x_9 + 0.672 \bullet x_{10} + 0.559 \bullet x_{11} + 0.814 \bullet x_{12} \quad (7)$$

Where: x_1, x_2, …, x_{12} are independent variables, which indicate the factor values of the slope, aspect, altitude, slope shape, land use, topographic relief, TRI, TWI, slope structure, lithology, distance to rivers, distance to faults; P is the probability of landslide susceptibility. The landslide susceptibility index is divided into five levels: Very High (5%), High (10%), Medium (15%), Low (20%), and Very Low (50%). The non-landslide samples for training are randomly selected only in the Very Low area. The preliminary susceptibility map (Fig 8) shows different classes of susceptibility (very high, high, moderate, low, very low and non-landslide) zone along both sides of the Yangtze River. The non-landslide samples are distributed throughout the study area, concentrated in the areas with high altitudes, steep slopes and few human engineering activities. Due to topographical and lithological constraints, landslides rarely develop in these areas. Therefore, the engineering geological conditions of the selected samples are quite different from those of the landslide, and they are more representative of landslide-free areas.

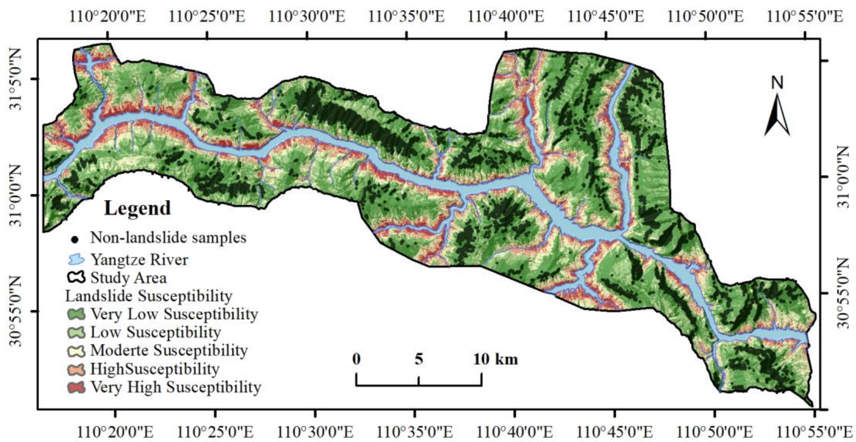

Fig.8 Preliminary susceptibility map and the distribution of non-landslide samples.

4.3.3 Parameter setting

4.3.3.1 Single models of CART and MLP

Maximum tree depth is the crucial parameter for CART Modelling. In this paper, a trial-and-error method determines the maximum tree depth of the CART as 8. Regarding MLP, the number of hidden layers and neurons affects its modeling accuracy. After multiple sets of tests, we find that a model structure of MLP with two hidden layers is suitable. The neuron number of the first and second layers are set to 8 and 25, respectively.

4.3.3.2 CART-Boosting

In the same way, we obtain the relationship between the parameters and model accuracy of CART-Boosting through multiple sets of trials (Fig. 9). Similarly with CART-Bagging, the accuracy of CART-Boosting first increases and then decreases with the sub-model number when the maximum tree depth is constant. In the case of fewer than 10 sub-models, the model accuracy increases with the maximum tree depth; While the sub-model number is larger than 10, the model accuracy showed a downward trend after the growth. Therefore, we set the maximum tree depth and the number of sub-models of CART-Boosting to 10 and 14, respectively.

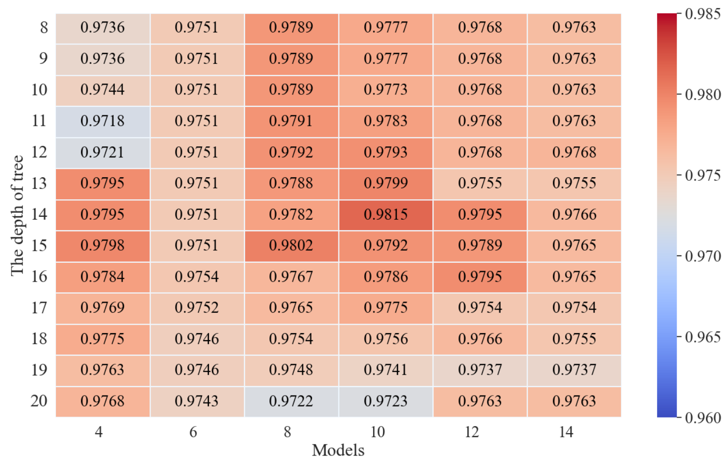

Fig. 9 Accuracy statistics of CART-Boosting with various parameters.

4.3.3.3 CART-Bagging

The number of sub-models and the maximum tree depth are the significant parameters for the CART-based ensemble learning models. To determine the optimal parameters, we obtain the relationship between the two parameters and the model accuracy of CART-bagging through multiple trials. As shown in Fig. 10, when the maximum tree depth is determined, the modeling accuracy increases with the number of the sub-model within a specific range. Similarly, when the number of sub-models is constant, and the maximum tree depth is less than 10, the modeling accuracy increases with the increase of maximum tree depth. Therefore, we set the maximum tree depth and the number of sub-models of CART-bagging as 8 and 10, respectively.

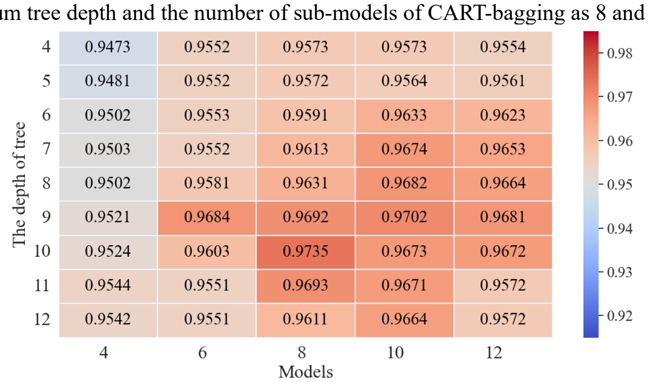

Fig. 10 Accuracy statistics of CART-Bagging with various parameters

4.3.3.4 MLP-Bagging and MLP-boosting.

The relationship between a sub-model number and the accuracy of MLP-based ensemble learning models is shown in Table 6. For MLP-Bagging and MLP-boosting, the model accuracy first increases and then decreases with the number of sub-models. For example, both models achieve the highest accuracy when

https://doi.org/10.5194/nhess-2023-44
Preprint. Discussion started: 13 April 2023

the sub-model number is 14. With this, we set the sub-model number of MLP-Bagging and MLP-Boosting models to 14.

Table 6 Statistics of the sub-model number and accuracy.

No. of sub-model	6	8	10	12	14	16	18	20
MLP-Bagging	0.9682	0.9740	0.9756	0.9764	0.9780	0.9767	0.9765	0.9761
MLP-Boosting	0.9823	0.9829	0.9848	0.9852	0.9857	0.9855	0.9853	0.9852

4.4 Landslide susceptibility mapping

The probability of landslide susceptibility is calculated by applying CART-Bagging, CART-Boosting, MLP-Bagging, MLP-Boosting, single CART, and single MLP models, respectively. According to the ratio of 0.5: 1: 1.5 : 2: 5, the probability value of landslide susceptibility is divided into five levels, namely Very High, High, Moderate, Low, and Very Low. The produced landslide susceptibility maps are presented in Fig. 11a-f. In addition, to verify the quality of the non-landslide samples selected by the LR constraint method, we choose a set of non-landslide samples under no constraint condition (the whole landslide-free area) for comparison. Similarly, these six models are used for LSM as well. The produced landslide susceptibility maps are shown in Fig. 11g-l, respectively.

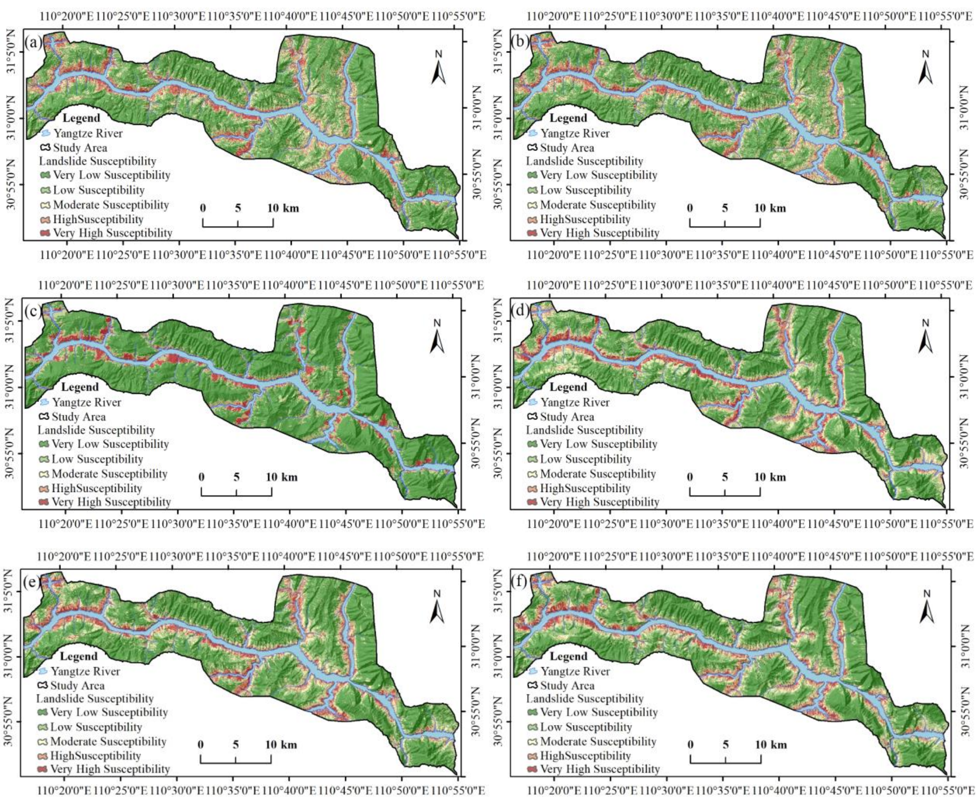

https://doi.org/10.5194/nhess-2023-44
Preprint. Discussion started: 13 April 2023

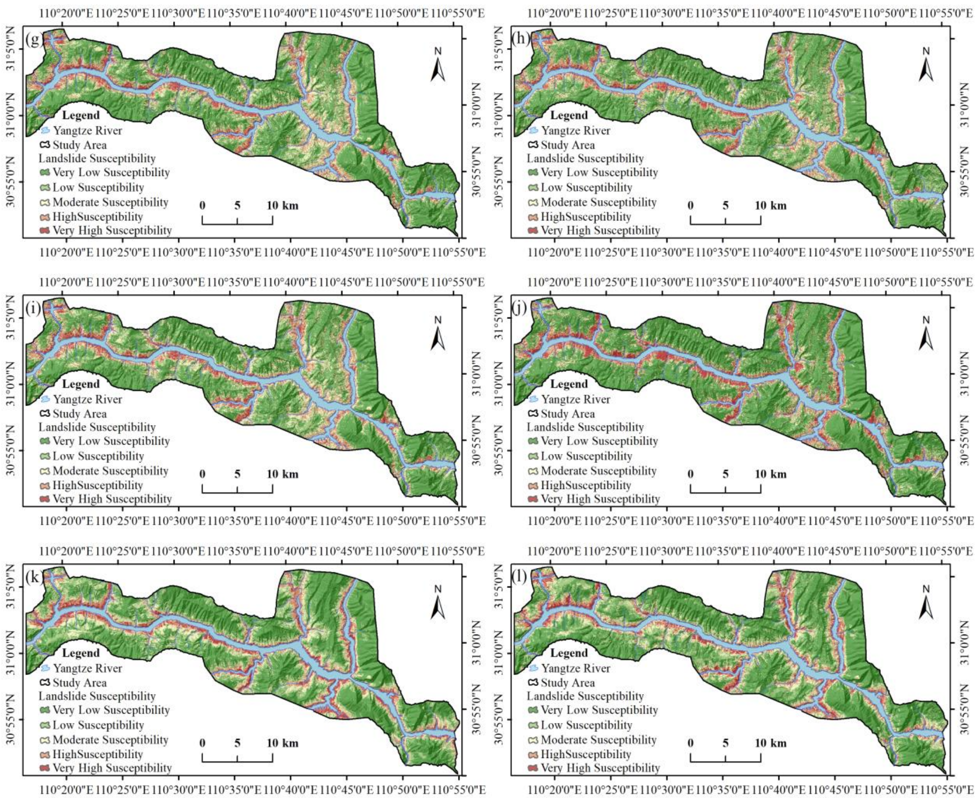

Fig. 11 Landslide susceptibility maps using different methods (a) LR-MLP-Boosting, (b) LR-MLP-Bagging, (c) LR-CART-Boosting, (d) LR-CART-Bagging, (e) LR-MLP, (f) LR-CART, (g) No-MLP-Boosting, (h) No-MLP-Bagging, (i) No-CART-Boosting, (j) No-CART-Bagging, (k) No-MLP, and (l) No-CART.

5 Discussion

5.1 The relationship between landslide development and the main factors

The statistics of information value (Table 1) and susceptibility maps (Fig. 11) indicate that the spatial development of landslides in this study area is mainly controlled by altitude, lithology, and distance to rivers. The widely distributed mudstone, marlstone, and weak strata, as well as the layered clastic rock strata containing weak interlayers, significantly reduced the sliding mass's strength, making the slope vulnerable to instability (Tang et al., 2019). In the study area, most landslides occur at a low altitude. An altitude of less than 240 m poses the most significant effect on landslide development, whose information value is the maximum of 1.49. This is because many human engineering activities occur in this area, where the thick loose deposits provide the material basis for landslide occurrence. The periodic fluctuation of reservoir water level significantly changes the hydrogeological conditions of bank slopes, and plenty of seepage-driven and buoyancy-driven landslides are triggered (Zhou et al., 2022). In the mountainous regions along the road,

Natural Hazards and Earth System Sciences
Open Access
Discussions

excessive rainfall enhances flow in the drainage, weakening the rock mass and triggering landslides. The statistics suggest that the closer the slope to the river, the more it is affected. When the distance to rivers is less than 300 m, its information value is high at 0.92. Additionally, it is to be noted that the information value method is a typical statistical method whose reliability depends on sufficient samples. The information value may need to be more accurate in the case of insufficient data.

5.2 performance comparison of the used algorithms

5.2.1 Machine learning algorithms

To verify the performance of the machine learning algorithms, we count the pixel distribution of four landslide susceptibility maps produced by LR-CART, LR-MLP, No-CART, and No-MLP (Table 7). The statistics indicate that the maps produced by these four models are the same. The landslide development law is consistent with the mapping results, which indicates that the LSM is reliable. Regarding LR-MLP, the higher the landslide susceptibility level, the higher the landslide ratio. 34.77% of the landslide pixels are located in the Very High susceptibility area, with the highest landslide ratio of 7.00.

Conversely, only 2.67% of the landslide pixels distributes in the Very Low susceptibility area, and the landslide ratio is 0.05. In the results of LR-MLP, the landslide ratio in the Very High susceptibility area is the highest at 6.89, where 35.57% of landslide pixels distribute in this area. The same characteristics are presented in the results of the No-MLP and No-CART models. The statistics suggest that MLP is slightly performed better than CART.

The receiver operating characteristic (ROC) curve is a commonly used performance evaluation method in landslide susceptibility assessment (Sun et al., 2021). The area under the ROC curve (AUC) is used to assess model performance, and the model with a larger AUC is considered better. As shown in Fig. 12, LR-MLP outperforms LR-CART, and their AUCs are 0.901 and 0.889, respectively. NO-MLP achieves better accuracy than NO-CART as well. The ROC curves suggest that both algorithms of MLP and CART perform excellently in LSM. We can infer MLP algorithm can more accurately establish the nonlinear relationship between landslide occurrence and its influencing factors than CART.

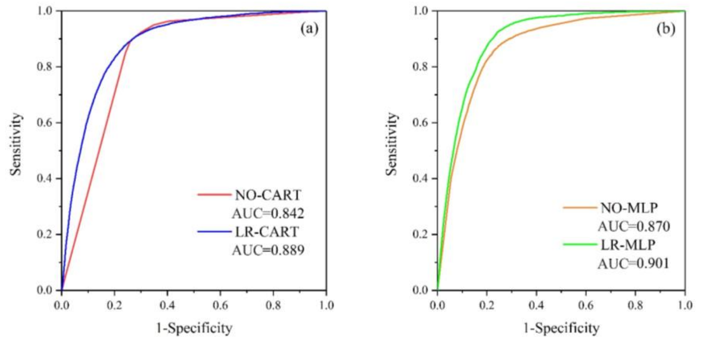

Fig. 12 ROC curves of single models: (a) LR- and NO-CART, and (b) LR- and NO-MLP.

Table 7 Statistical results of susceptibility zoning.

Levels	Landslide pixles		Domain pixles		Ratio
	No.	% (a)	No.	% (b)	(a/b)
No-CART					
Very Low	861	3.56	353,136	50.55	0.07
Low	1,506	6.22	138,069	19.76	0.31
Moderate	4,882	20.18	101,150	14.48	1.39
High	8,393	34.69	69,174	9.90	3.50
Very High	8,553	35.35	37,117	5.31	6.65
No-MLP					
Very Low	846	3.35	351,927	50.37	0.07
Low	1,666	6.89	134,798	19.29	0.36
Moderate	5,174	21.38	108,194	15.49	1.38
High	8,250	34.09	68,527	9.81	3.48
Very High	8,259	34.14	35,200	5.04	6.77
LR-CART					
Very Low	645	2.67	341,817	48.93	0.05
Low	1,543	6.38	145,048	20.76	0.30
Moderate	4,674	19.32	107,442	15.38	1.26
High	8,726	36.07	68,256	9.77	3.69
Very High	8,607	35.57	36,083	5.16	6.89
LR-MLP					
Very Low	652	2.69	352,147	50.4	0.05
Low	1,408	5.82	136,945	19.6	0.30
Moderate	4,869	20.12	107,515	15.39	1.31
High	8,854	36.59	67,333	9.64	3.80
Very High	8,412	34.77	34,706	4.97	7.00

5.2.2 Ensemble learning algorithms

The result statistics of the eight coupling models are shown in Table 8. In the landslide susceptibility map produced by LR-MLP-Boosting, 43.75% of the landslide pixels are distributed in the Very High susceptibility area. Its landslide ratio is the highest of 8.594, while the Very Low susceptibility area is the lowest 0.028. LR-MLP-Boosting not only achieves the best prediction accuracy but also has the lowest false negative error which may lead to catastrophic losses. Higher landslide ratios in Very High susceptibility areas and lower landslide ratios in Very Low susceptibility areas suggest that the model has better performance. The comparison results indicate that LR-MLP-Boosting performs better than LR-CART-Boosting, and LR-

https://doi.org/10.5194/nhess-2023-44
Preprint. Discussion started: 13 April 2023

Natural Hazards and Earth System Sciences Discussions

MLP-Bagging outperforms LR-CART-Bagging. The same comparison results are presented in the results of the No-MLP-Boosting, No-MLP-Bagging, No-CART-Boosting, and No-CART-Bagging models.

Table 8 Statistical results of each landslide susceptibility zoning.

Levels	Landslide pixels		Domain pixels		Ratio
	No	% (a)	No	% (b)	(a/b)
LR-MLP-Boosting					
Very Low	346	1.43	352,156	50.41	0.028
Low	706	2.92	135,816	19.44	0.150
Moderate	3,222	13.32	105,327	15.08	0.883
High	9,336	38.59	69,792	9.99	3.863
Very High	10,585	43.75	35,555	5.09	8.597
LR-MLP-Bagging					
Very Low	423	1.75	359,283	51.43	0.034
Low	933	3.86	131,112	18.77	0.205
Moderate	4,185	17.30	105,520	15.10	1.145
High	8,998	37.19	68,320	9.78	3.803
Very High	9,656	39.91	34,411	4.93	8.103
LR-CART-Boosting					
Very Low	394	1.63	364,801	52.22	0.031
Low	770	3.18	122,823	17.58	0.181
Moderate	3,829	15.83	107,890	15.44	1.025
High	9,006	37.22	67,320	9.64	3.863
Very High	10,196	42.14	35,812	5.13	8.221
LR-CART-Bagging					
Very Low	413	1.71	342,258	48.99	0.035
Low	1,105	4.57	145,233	20.79	0.220
Moderate	3,786	15.65	107,928	15.45	1.013
High	8,883	36.71	67,105	9.61	3.820
Very High	10,008	41.36	36,122	5.17	8.000
No-MLP-Boosting					
Very Low	595	2.46	342,258	51.43	0.048
Low	929	3.84	145,233	18.77	0.205
Moderate	4,124	17.04	107,928	15.07	1.131
High	8,834	36.51	67,105	9.78	3.735
Very High	9,713	40.14	36,122	4.96	8.094
No-MLP-Bagging					
Very Low	601	2.48	353,804	50.64	0.049
Low	1,089	4.50	132,710	18.99	0.237
Moderate	4,034	16.67	108,589	15.54	1.073
High	8,707	35.99	67,991	9.73	3.698
Very High	9,764	40.36	35,552	5.09	7.930
No-CART-Boosting					
Very Low	623	2.57	352,231	50.16	0.051
Low	1,106	4.57	135,474	19.39	0.236
Moderate	4,121	17.03	107,995	15.46	1.102
High	8,786	36.31	67,976	9.73	3.732
Very High	9,559	39.51	34,970	5.01	7.893
No-CART-Bagging					
Very Low	622	2.57	342,258	48.99	0.050
Low	1,340	5.54	145,233	20.79	0.260
Moderate	3,750	15.50	107,928	15.45	1.000
High	8,688	35.91	67,105	9.61	3.740
Very High	9,795	40.48	36,122	5.17	7.830

https://doi.org/10.5194/nhess-2023-44
Preprint. Discussion started: 13 April 2023

Natural Hazards and Earth System Sciences
Open Access
Discussions

We also utilize the ROC curves to quantify the performance of the coupling models. The same conclusion about the performance ranking of the coupled models can be drawn from the ROC Curves (Fig. 13). LR-MLP-Boosting achieves the best prediction accuracy with the highest AUC of 0.985. Apparently, the coupling models outperform the single machine learning models. Boosting and Bagging improve the accuracy of LR-MLP by 0.085 and 0.077, respectively, while improving the accuracy of LR-CART by 0.092 and 0.084, respectively (Table 9). Accuracy improvement from Boosting is more significant than the improvement from Bagging. In Boosting method, the prediction of all the sub-models was sequentially integrated into the training process to achieve the final results (Fig. 3). However, it is parallel to the Bagging method (Fig. 4). The boosting method is more effective at reducing the deviation and variance, which enhances the prediction ability of the coupling model.

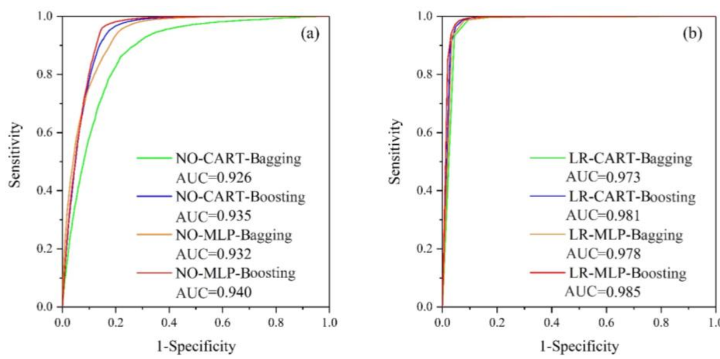

Fig. 13 ROC curves of coupling models: (a) no constraint sampling and (b) LR constrained sampling

Table 9 Statistics of modelling accuracy.

Single model	Original	Bagging		Boosting	
	AUC	AUC	Improvement	AUC	Improvement
No sampling					
CART	0.842	0.926	0.084	0.935	0.093
MLP	0.870	0.932	0.062	0.940	0.070
LR sampling					
CART	0.889	0.973	0.084	0.981	0.092
MLP	0.901	0.978	0.077	0.986	0.085

5.3 The advantages of the proposed method for non-landslide sampling

High-quality non-landslide samples are critical to the performance improvement of LSM. We use two methods for non-landslide sampling, and two single models and four coupling models for susceptibility mapping are established using selected samples. As shown in the ROC curves and statistics (Figs. 12 and 13, Tables 8 and 9), all the LR- models achieve a better performance than the corresponding NO- models. It indicates that the application of the LR model to constrain the selection range of non-landslide samples can

https://doi.org/10.5194/nhess-2023-44
Preprint. Discussion started: 13 April 2023

effectively improve sample quality.

Many machine learning methods can produce more accurate initial susceptibility maps to constrain the range of non-landslide sampling. However, as reported in earlier studies (Zhou et al., 2018; Yang et al., 2021; Sun et al., 2022), the performance of machine learning methods varies in regions, and high-quality data is required. As a result, a poor prediction may occur in some landslide-prone regions. Due to the simplicity of operation, high accuracy and stable performance, LR is widely used and consistently achieves acceptable results. In comparison, LR is a better choice to ensure the generalization of the non-landslide sampling method.

The non-landslide pixels obtained by random sampling under no constraint conditions may have engineering geological conditions prone to landslides. The mixing of these pixels will reduce the quality of non-landslide samples. In addition, the engineering geological conditions that inhibit the occurrence of landslides are diverse. Some non-landslide sampling range constraint methods, such as the low-slope method, cannot select non-landslide samples with different geological conditions. Therefore, it may limit the improvement of modelling accuracy. LR model produces an initial susceptibility map, and non-landslide samples are only selected from the Very Low susceptibility areas. This method can effectively avoid the mis-selection of samples in landslide-prone areas and keep the diversity of non-landslide sample characteristics. In general, our proposed non-landslide sampling method is conducive to improving LSM performance and can be applied worldwide.

6 Conclusion

Our detailed analysis is based on two single models (CART and MLP) and four coupling models (CART-Bagging, CART-Boosting, MLP-Bagging, and MLP-Boosting) to study the landslide susceptibility map using two kinds of non-landslide samples. We quantitatively analyze the relationship between landslide spatial development and each causal factor. We have considered twelve controlling parameters as inputs for LSM after multi-collinearity analysis. We found that the altitude (<240 m) and distance to rivers (<300 m) emerged as important factors for the cause of landslides in the study area. Their information values are the highest at 1.49 and 0.92, respectively. LR-MLP-Boosting achieves the highest prediction accuracy with an AUC of 0.985. The accuracy of the comparison indicates that MLP performs better than CART. The coupling models outperform the corresponding single models and Boosting algorithm performs better than the Bagging algorithm. High-quality non-landslide samples enhance the accuracy of LSM. They can be effectively obtained by using the LR model to constrain its selection range. The non-landslide samples selected from the low susceptibility area are of higher quality than those selected from the entire landslide-free area. LR is a reliable method to generate a preliminary susceptibility map to determine the Very Low susceptibility area. The results will be of great help to the community and to the scientists to monitor the susceptible locations and to get an early information about the occurrence of landslide event to minimize loss of life and damages.

Acknowledgements

This research is funded by the National Natural Science Foundation of China (No. 41907253 and No. 41702330) and the Key Research and Development Program of Hubei Province (No. 2021BCA219). The first author would like to thank the China Scholarship Council for funding his research at the German Research Centre for Geosciences.

References

[1] Abdo H G. Assessment of landslide susceptibility zonation using frequency ratio and statistical index: a case study of Al-Fawar basin, Tartous, Syria[J]. International Journal of Environmental Science and Technology, 2022, 19(4): 2599-2618.

[2] Aditian A, Kubota T, Shinohara Y. Comparison of GIS-based landslide susceptibility models using frequency ratio, logistic regression, and artificial neural network in a tertiary region of Ambon, Indonesia[J]. Geomorphology, 2018, 318: 101-111.

[3] Al-najjar Han, Pradham B.. Spatial Landslide Susceptibility Assessment Using Machine Learning Techniques Assisted by Additional Data Created with Generative Adversarial Networks[J]. Geoscience Frontiers, 2021, 12: 625-637.

[4] Breiman L. Stacked Regressions[J]. Machine Learning 1996, 24(1): 49-64.

[5] Bui DT., Tsangaratos P., Nguyen VT., et al.. Comparing the prediction performance of a deep learning neural network model with conventional machine learning models in landslide susceptibility assessment[J]. Catena, 2020, 188.

[6] Chen Tao, Zhong Ziying, Niu Ruiqing, et al.. Mapping Landslide Susceptibility Based on Deep Belief Network[J]. Geomatics and Information Science of Wuhan University, 2020, 45(11): 1809-1817.

[7] Chen W., Reza H., Kornejady A.. Landslide spatial modeling: Introducing new ensembles of ANN, MaxEnt, and SVM machine learning techniques[J]. Geoderma, 2017, 305: 314-327.

[8] Chen W., Lei X.X., Chakrabortty R., et al.. Evaluation of different boosting ensemble machine learning models and novel deep learning and boosting framework for head-cut gully erosion susceptibility[J]. Journal of Environmental Management, 2021, 284.

[9] Dai F.C., Lee C.F., Li J., et al. Assessment of Landslide Susceptibility on the Natural Terrain of Lantau Island, Hong Kong[J]. Environmental Geology, 2001, 40(3): 381-391.

[10] Di Napoli M, Carotenuto F, Cevasco A, et al. Machine learning ensemble modelling as a tool to improve landslide susceptibility mapping reliability[J]. Landslides, 2020, 17(8): 1897-1914.

[11] Fang, Z., Wang, Y., Niu R., et al., 2021. Landslide Susceptibility Prediction Based on Positive Unlabeled Learning Coupled with Adaptive Sampling[J]. IEEE Journal of Selected Topics in Applied Earth Observations and Remote Sensing,

https://doi.org/10.5194/nhess-2023-44
Preprint. Discussion started: 13 April 2023

14: 11581-11592. https://doi.org/10.1109/JSTARS.2021.3125741.

[12] Fang Z, Wang Y, Peng L, et al. A comparative study of heterogeneous ensemble-learning techniques for landslide susceptibility mapping[J]. International Journal of Geographical Information Science, 2021, 35(2): 321-347.

[13] Gardner M W, Dorling S R. Artificial neural networks (the multilayer perceptron)—a review of applications in the atmospheric sciences[J]. Atmospheric environment, 1998, 32(14-15): 2627-2636.

[14] Guo Zizheng, Yin Kunlong, Huang Faming, et al.. Evaluation of landslide susceptibility based on landslide classification and weighted frequency ratio model[J]. Chinese Journal of Rock Mechanics and Engineering, 2019, 38(2): 287-300.

[15] Hecht-Nielsen R. Kolmogorov's mapping neural network existence theorem[C]. Proceedings of the international conference on Neural Networks. New York: IEEE Press,1987, 3:11-14.

[16] Huang B.L., Yin Y.P., Liu G.N., et al.. Analysis of waves generated by Gongjiafang landslide in Wu Gorge, three Gorges reservoir, on November 23, 2008[J]. Landslides, 2012, 9(3): 395-405.

[17] Huang F.M, Yin K.L, Tao H., et al.. Influencing Factor Analysis and Displacement Prediction in Reservoir Landslides-A Case Study of Three Gorges Reservoir (China)[J]. Tehnicki Vjesnik-Technical Gazette, 2016, 23(2): 617-626.

[18] Huang F.M., Yin K.L., Huang J.S., et al.. Landslide Susceptibility Mapping Based on Self-Organizing-Map Network and Extreme Learning Machine[J]. Engineering Geology, 2017, 223: 11-22.

[19] Huang Faming, Yin Kunlong, Jiang Shuihua, et al.. Landslide susceptibility assessment based on clustering analysis and support vector machine[J]. Chinese Journal of Rock Mechanics and Engineering, 2018, 37(1): 156-167.

[20] Huang Faming, Ye Zhou, Yao Chi, et al. Uncertainties of Landslide Susceptibility Prediction: Different Attribute Interval Divisions of Environmental Factors and Different Data-based Models[J]. Earth Science, 2020, 45(12): 4535-4549.

[21] Huang Y., Zhao L.. Review on landslide susceptibility mapping using support vector machines[J]. Catena, 2018, 165: 520-529.

[22] Kalantar B, Pradhan B, Naghibi S A, et al. Assessment of the effects of training data selection on the landslide susceptibility mapping: a comparison between support vector machine (SVM), logistic regression (LR) and artificial neural networks (ANN)[J]. Geomatics, Natural Hazards and Risk, 2018, 9(1): 49-69.

[23] Kayastha P., Dhital MR., De Smedt F.. Application of the analytical hierarchy process (AHP) for landslide susceptibility mapping: a case study from the Tinau watershed, west Nepal[J]. Computers and Geoscience, 2013, 52: 398-408.

[24] Kavzouglu, T., Sahin, E.K., Colkesen, I.. Landslide Susceptibility Mapping Using GIS-based Multi-criteria Decision Analysis, Support Vector Machines, and Logistic Regression[J]. Landslides, 2014, 11(3): 425−4 39. https://doi.org/ 10.1007/s10 346-013-0391-7.

[25] Kornejady, A., Onegh, M., Bahraemand, A.. Landslide Susceptibility Assessment Using Maximum Entropy Model with Two Different Data Sampling Methods[J]. Catena, 2017,152: 144-162.

[26] Jacobs, Liesbet, et al.. Regional Susceptibility Assessments with Heterogeneous Landslide Information: Slope unit-vs. Pixel-based Approach[J]. Geomorphology, 2020 356(2020): 107084.

[27] Li Songlin, Xu Qiang, Tang Minggao, et al. Study on Spatial Distribution and Key Influencing Factors of Landslides in Three Gorges Reservoir Area[J]. Earth Science, 2020, 45(1): 341-354.

https://doi.org/10.5194/nhess-2023-44
Preprint. Discussion started: 13 April 2023

Natural Hazards and Earth System Sciences
Open Access
EGU
Discussions

[28] Liu Xuejun, Zhang Ping, Zhu Ying. Suitable Window Size of Terrain Parameters Derived from Grid-based DEM[J]. Acta Geodaetica et Cartographica Sinica, 2009, 38(3): 264-271.

[29] Lin Rongfu, Liu Jiping, Xu Shenghua, et al.. Evaluation method of ladslide susceptibility based on random forest weighted information[J]. Science of Surveying and Mapping, 2020, 45(12): 131-138.

[30] Liu Lei, Yin Kunlong, Xu Yong, et al. Evaluation of Regional Landslide Stability Considering Rainfall and Variation of Water Level of Reservoir[J]. Chinese Journal of Rock Mechanics and Engineering, 2018, 37(2): 403-414

[31] Long J, Liu Y, Li C, et al. A novel model for regional susceptibility mapping of rainfall-reservoir induced landslides in Jurassic slide-prone strata of western Hubei Province, Three Gorges Reservoir area[J]. Stochastic Environmental Research and Risk Assessment, 2021, 35(7): 1403-1426.

[32] Lv L, Chen T, Dou J, et al. A hybrid ensemble-based deep-learning framework for landslide susceptibility mapping[J]. International Journal of Applied Earth Observation and Geoinformation, 2022, 108: 102713.

[33] Meena, S. R., Puliero, S., Bhuyan, K., et al. Assessing the importance of conditioning factor selection in landslide susceptibility for the province of Belluno (region of Veneto, northeastern Italy)[J]. Natural hazards and earth system sciences, 2022, 22, 1395-1417.

[34] Moore I D, Grayson R B, Ladson A R. Digital Terrain Modelling-A Review of Hydrological, Geomorphological, and Biological Applications[J]. Hydrological Process, 1991, 5(1): 3-30.

[35] Pham B.T., Bui D.T., Prakash I., et al. Hybrid Integration of Multilayer Perceptron Neural Networks and Machine Learning Ensembles for Landslide Susceptibility Assessment at Himalayan Area (India) Using GIS[J]. Catena, 2017, 149: 52-63.

[36] Pham B T, Nguyen-Thoi T, Qi C, et al. Coupling RBF neural network with ensemble learning techniques for landslide susceptibility mapping[J]. Catena, 2020, 195: 104805.

[37] Pham B T, Jaafari A, Nguyen-Thoi T, et al. Ensemble machine learning models based on Reduced Error Pruning Tree for prediction of rainfall-induced landslides[J]. International Journal of Digital Earth, 2021, 14(5): 575-596.

[38] Roy, P., Martha, T.R., Vinod Kumar, K., et al. Cluster landslides and associated damage in the Dima Hasao district of Assam, India due to heavy rainfall in May 2022 [J]. Landslides, 2023, 20(1): 97-109.

[39] Sabokbar HF., Roodposhti MS., Tazik E.. Landslide susceptibility mapping using geographically-weighted principal component analysis[J]. Geomorphology, 2014, 226: 15-24.

[40] Shahabi H., Hashim M.. Landslide susceptibility mapping using GIS-based statistical models and Remote sensing data in tropical environment[J]. Science Report, 2015, 5(9899).

[41] Sun, D., Wen, H., Zhang, Y. and Xue, M., 2021. An optimal sample selection-based logistic regression model of slope physical resistance against rainfall-induced landslide. Natural Hazards, 105(2), pp.1255-1279.

[42] Sun D, Gu Q, Wen H, et al. Assessment of landslide susceptibility along mountain highways based on different machine learning algorithms and mapping units by hybrid factors screening and sample optimization[J]. Gondwana Research, 2022.

[43] Tang H.M., Wasowski J., Juang C.H.. Geohazards in the three Gorges Reservoir Area, China Lessons learned

https://doi.org/10.5194/nhess-2023-44
Preprint. Discussion started: 13 April 2023

from decades of research[J]. Engineering Geology, 2019, 261:105267.

[44] Tanyu B.F, Abbaspour A., Alimohammadlou Y, et al. Landslide susceptibility analyses using Random Forest, C4. 5, and C5. 0 with balanced and unbalanced datasets[J]. Catena, 2021, 203: 105355.

[45] Tian Nai Man, Lan Heng xing, Wu Yuming , et al. Performance comparison of BP artificial neural network and CART decision tree model in landslide susceptibility prediction[J]. Journal of Geo-information Science, 2020, 22(12): 2304-2316.

[46] Wang F, Zhang Y, Huo Z, et al. Mechanism for the rapid motion of the Qianjiangping landslide during reactivation by the first impoundment of the Three Gorges Dam reservoir, China[J]. Landslides, 2008, 5(4): 379-386.

[47] Wang Jiajia, Yin Kunlong, Xiao Lili. Landslide Susceptibility Assessment Based on GIS and Weighted Information Value:A Case Study of Wanzhou District, Three Gorges Reservoir. Chinese Journal of Rock Mechanics and Engineering, 2014, 33(4): 797-808.

[48] Wu Y.L., Ke Y.T., Chen Z., et al.. Application of alternating decision tree with AdaBoost and bagging ensembles for landslide susceptibility mapping[J]. Catena, 2020, 187: 1-17.

[49] Xie Quanmin, Bian Xiang, Xia Yuanyou. Systematic analysis of risk evaluation of landslide hazard[J]. Rock and Soil Mechanics, 2005, 26(1): 71-74.

[50] Yang C, Liu L L, Huang F, et al. Machine learning-based landslide susceptibility assessment with optimized ratio of landslide to non-landslide samples[J]. Gondwana Research, 2022.

[51] Yang Haiwei, Cao Kefeng. Application of Information Method to Slope Stability Zoning[J]. Yangtze River, 2003, 34(10).

[52] Yang Yonggang, Yin Kunlong, Zhao Haiyan, et al.. Landslide susceptibility evaluation for township units of bank section in wanzhou distict based on C5.0 decision tree and K-means cluster model[J]. Geological science and technology information, 2019, 38(6): 189-197.

[53] Ye Runqing, Fu Xiaolin, Guo Fei, et al. 2021. Deformation characteristics and mechanism analysis of geological hazards during the operation period of Three Gorges Reservoir[J]. Journal of Engineering Geology, 29(3): 680-692.

[54] Yin Yueping, Zhang Chenyang, Yan Hui, et al. Research on seepage stability and prevention design of landslide during impoundment operation of the Three Gorges Reservoir, China[J/OL]. Chinese Journal of Rock Mechanics and Engineering.

[55] Yin, K.L., Zhang, Y., Wang, Y.. A Review of Landslide-generated Waves Risk and Practice of Management of Hazard Chain Risk from Reservoir Landslide[J]. Bulletin of Geological Science and Technology, 2022, 41(2): 1-12.

[56] Youssef A.M., Pourghasemi H.R., Pourtachi Z. S., et al. Landslide Susceptibility Mapping Using Random Forest, Boosted Regression Tree, Classification and Regression Tree, and General Linear Models and Comparison of Their Performance at Wadi Tayyah Basin, Asir Region, Saudi Arabia[J]. Landslides, 2016, 13: 839-856.

[57] Yu L.B., Cao Y., Zhou C., et al. Landslide Susceptibility Mapping Combining Information Gain Ratio and Support Vector Machines: A Case Study from Wushan Segment in the Three Gorges Reservoir Area, China[J]. Applied Sciences, 2019, 9(22): 4756.

[58] Yu Xianyu, Hu Youjian, Niu Ruiqing, et al. Research on the Method to Select Landslide Susceptibility Evaluation Factors

https://doi.org/10.5194/nhess-2023-44
Preprint. Discussion started: 13 April 2023

Natural Hazards and Earth System Sciences
Open Access
Discussions

Based on RS-SVM Model[J]. Geography and Ceo-Information Science, 2016, 32(3): 23-28.

[59] Yu Xianyu, Zhang Kaixiang, Song Yingxu, et al. Study on landslide susceptibility mapping based on rock–soil characteristic factors. Sci Rep 11, 15476 (2021).

[60] Zheng Yingkai, Chen Jianguo, Wang Chengbin, et al.. Application of certainty factor and random fo re sts model in landslide susceptibility evaluation in Mangshi City, Yunnan Province[J]. Bulletin of Geological Science and Technology, 2020, 39(6): 131-144.

[61] Zhou Chao, Yin Kunlong, Cao Ying, et al.. Displacement prediction of step-like landslide based on the response of inducing factors and support vector machine[J]. Chinese Journal of Rock Mechanics and Engineering, 2015, 34(Supp.2): 4132-4139.

[62] Zhou C, Yin K, Cao Y, et al. Landslide susceptibility modeling applying machine learning methods: A case study from Longju in the Three Gorges Reservoir area, China[J]. Computers & Geosciences, 2018, 112: 23-37.

[63] Zhou C, Yin K, Cao Y, et al. Displacement prediction of step-like landslide by applying a novel kernel extreme learning machine method[J]. Landslides, 2018, 15(11): 2211-2225.

[64] Zhou Chao. Landslide Identification and Prediction with the Application of Time Series InSAR[D]. Wuhan: China University of Geosciences, 2018.

[65] Zhou C, Cao Y, Yin K, et al. Landslide characterization applying sentinel-1 images and InSAR technique: The Muyubao landslide in the three Gorges Reservoir Area, China[J]. Remote Sensing, 2020, 12(20): 3385.

[66] Zhou Chao, Yin Kunlong, Cao Ying, et al.. Landslide susceptibility assessment by applying the coupling method of radial basis neural network and adaboost: a case study from the three gorges reservoir area[J]. Earth Science, 2020, 45(6): 1865-1876.

[67] Zhou Chao, Ying Cao, Kunlong Yin, et al.. Characteristic comparison of seepage-driven and buoyancy-driven landslides in Three Gorges Reservoir area, China[J]. Engineering Geology, 2022, 301: 106590.